PAPER

Solubility of cholesterol in lipid membranes and the formation of immiscible cholesterol plaques at high cholesterol concentrations†

Matthew A. Barrett,‡[a] Songbo Zheng,[a] Laura A. Toppozini,[a] Richard J. Alsop,[a] Hannah Dies,[a] Aili Wang,[a] Nicholas Jago,[a] Michael Moore[a] and Maikel C. Rheinstädter*[ab]

The molecular in-plane and out-of-plane structure of dimyristoylphosphatidylcholine (DMPC) membranes containing up to 60 mol% of cholesterol was studied using X-ray diffraction. Up to 37.5 mol% cholesterol could be dissolved in the membranes, resulting in a disordered lateral membrane structure. Highly ordered cholesterol structures were observed at cholesterol concentrations of more than 40 mol% cholesterol. These structures were characterized as immiscible cholesterol plaques, *i.e.*, bilayers of cholesterol molecules coexisting with the lipid bilayer. The cholesterol molecules were found to form a monoclinic structure at 40 mol% cholesterol, which transformed into a triclinic arrangement at the highest concentration of 60 mol%. Monoclinic and triclinic structures were found to coexist at cholesterol concentrations between 50 and 55 mol%.

Cholesterol is an essential structural component of eukaryotic cell membranes capable of modulating their permeability and molecular organization. It is either obtained from foods of animal origin, or synthesized in the endoplasmic reticulum, a multifold membranous structure that is also capable of producing phospholipids, including different types of membranes.[1] Higher sterols are universally present in large amounts (20–30 mol%) in the plasma membranes of all eukaryotic cells: cholesterol in animals, ergosterol in yeast and fungi, phytosterols in plants, and fucosterol in algae,[2] making sterols by any comparison, the single most abundant molecule in plasma membranes. Cholesterol is known to order fluid lipid bilayers, providing for low passive permeability and increased mechanical strength.[3,4] These effects have been demonstrated by a large body of literature for a wide range of model membranes.[5]

Cholesterol is speculated to be distributed non-randomly in domains in biological and model membranes.[6] This can result in the formation of so-called *rafts*, nano- to micrometer sized transient functional domains, which are thought to take part in membrane-associated events such as signal transduction, cell adhesion, signalling, cell trafficking and lipid/protein sorting.[7–24] Immiscible cholesterol domains were observed at high cholesterol concentrations.[25–27] These alterations in membrane structure and organization are speculated to have significance in early stages of atherosclerosis, as precursor of atherosclerosis plaques.[25]

The interaction between lipids and cholesterol and the formation of cholesterol domains and their molecular structure was studied previously. The Leiserowitz group conducted seminal experiments to determine the lateral structure of monolayer and bilayer films at the air–water interface.[28–33] Cholesterol domains with monoclinic and triclinic crystalline structures were observed in these studies using X-ray diffraction. X-ray reflectivity experiments in muscle cell plasma membranes indicated the presence of an immiscible cholesterol domain with a unit cell periodicity of 34 Å, consistent with a cholesterol monohydrate tail-to-tail bilayer.[25,26] Evidence for immiscible cholesterol bilayer domains in phospholipid bilayers was presented from electron paramagnetic resonance (EPR).[27] By combining out-of-plane (reflectivity) and in-plane X-ray diffraction we investigated the formation of cholesterol domains in model phospholipid bilayers and determined the corresponding lateral and out-of-plane structure of the membrane/cholesterol complexes simultaneously.

We conducted a series of high-resolution X-ray diffraction experiments to determine the molecular structure of dimyristoylphosphatidylcholine membranes containing different amounts of cholesterol. Schematics of lipid and cholesterol molecules and the corresponding membrane structures are

[a]*Department of Physics and Astronomy, McMaster University, Hamilton, ON, Canada. E-mail: rheinstadter@mcmaster.ca*

[b]*Canadian Neutron Beam Centre, National Research Council Canada, Chalk River, ON, Canada*
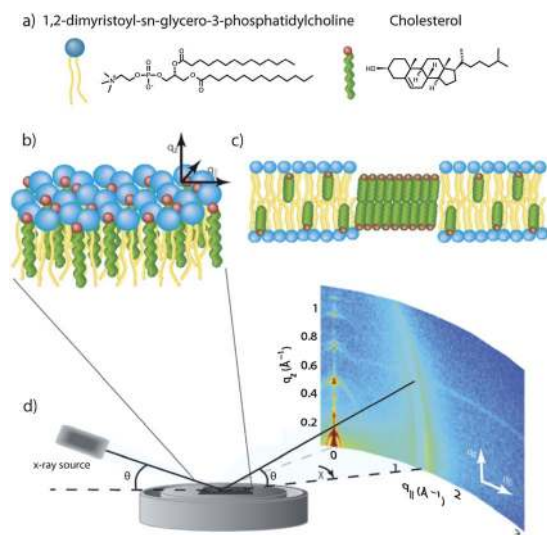
Fig. 1 (a) Schematic representations of dimyristoylphosphatidylcholine (DMPC) and cholesterol molecules. (b) Model of a membrane containing cholesterol. The cholesterol molecules take an upright position in bilayers made of saturated lipids. (c) Immiscible cholesterol bilayer coexisting with the membrane at high cholesterol concentrations. (d) Schematic diagram of the X-ray scattering experiment.

shown in Fig. 1(a), (b) and (c). Highly oriented, solid supported multi-lamellar membrane stacks containing up to 60 mol% of cholesterol were prepared on silicon wafers. By using highly oriented membranes the in-plane and out-of-plane structure of

the bilayers could be determined. At low concentrations, the addition of cholesterol led to a disordered membrane structure. Up to 37.5 mol% cholesterol could be dissolved in the membranes before immiscible cholesterol patches, *i.e.*, coexisting lamellar cholesterol bilayers, were observed. The cholesterol molecules in these patches were found to undergo a structural phase transition from a monoclinic into a triclinic bilayer phase at the highest cholesterol concentrations.

Results

Thirteen different membrane complexes of dimyristoylphosphatidylcholine (DMPC) with concentrations of cholesterol molecules from 0 mol% to 60 mol% cholesterol were prepared for this study, as detailed in the Materials and methods section and listed in Table 1. Fig. 2 shows 2-dimensional X-ray intensity maps for selected concentrations: (a) pure DMPC, (b) 2 mol% cholesterol, (c) 20 mol% cholesterol, (d) 37.5 mol% cholesterol, (e) 40 mol% cholesterol and (f) 50 mol% cholesterol. As depicted in Fig. 1(d), the samples were oriented such that the $q_{\parallel}$ axis probed lateral membrane structure and the perpendicular axis, q_z, probed out-of-plane structure of the multi-lamellar membrane complexes. Data were collected at $T = 20$ °C and 50% relative humidity, in a de-hydrated membrane state to emphasize the structural features in the X-ray scattering experiment. Fully hydrated liquid crystalline samples are generally assumed to best mimic physiologically relevant

Table 1 List of all samples prepared for this study and their molecular composition. Unit cell dimensions, area per lipid and cholesterol molecules and the lamellar spacings for lipid and cholesterol bilayers (d_z^{lipid} and d_z^{chol}) are given. See text for details

| Sample	DMPC (mol%)	Cholesterol (mol%)	Unit Cell	Area per lipid (Å²)	d_z^{lipid} (Å)	Area per cholesterol (Å²)	d_z' (Å)	d_z^{chol} (Å)
1	100	0	Head-groups: $a_H = 8.77$ Å, $b_H = 9.31$ Å, $\gamma_H = 90°$ Lipid tails: $a_T = 4.97$ Å, $b_T = 8.25$ Å, $\gamma_T = 94.18°$	40.84 ± 0.1	52.6 ± 0.1	—	—	—
2	98	2	Lipid tails: $a_T = 4.91$ Å, $\gamma_T = 120°$	41.8 ± 0.4	53.3 ± 0.1	—	—	—
3	97	3	Lipid tails: $a_T = 4.91$ Å, $\gamma_T = 120°$	41.8 ± 0.4	54.9 ± 0.1	—	—	—
4	90	10	Lipid tails: $a_T = 4.94$ Å, $\gamma_T = 120°$	42.3 ± 0.6	51.5 ± 0.1	—	—	—
5	80	20	Lipid tails: $a_T = 5.01$ Å, $\gamma_T = 120°$	43.5 ± 0.8	50.0 ± 0.1	—	—	—
6	70	30	Lipid tails: $a_T = 5.12$ Å, $\gamma_T = 120°$	45.4 ± 0.9	50.5 ± 0.1	—	—	—
7	65	35	Lipid tails: $a_T = 5.18$ Å, $\gamma_T = 120°$	46.5 ± 1.0	48.8 ± 0.1	—	—	—
8	62.5	37.5	Lipid tails: $a_T = 5.25$ Å, $\gamma_T = 120°$	47.8 ± 1.1	48.8	—	—	—
9	60	40	Lipid tails: $a_T = 4.48$ Å, $\gamma_T = 120°$ Chol monoclinic: $a = 10.70$ Å, $b = 8.60$ Å, $\gamma = 103.0°$	34.8 ± 0.1	50.9 ± 0.1	44.83 ± 0.1	41.7 ± 0.1	32.5 ± 0.3
10	55	45	Lipid tails: $a_T = 4.48$ Å, $\gamma_T = 120°$ Chol monoclinic: $a = 10.70$ Å, $b = 8.60$ Å, $\gamma = 103.0°$	34.8 ± 0.1	50.3 ± 0.1	44.83 ± 0.1	39.5 ± 0.1	28.7 ± 0.3
11	50	50	Lipid tails: $a_T = 4.68$ Å, $\gamma_T = 120°$ Chol monoclinic: $a = 10.30$ Å, $b = 8.50$ Å, $\gamma = 101.0°$ Chol triclinic: $a = b = 14.1$ Å, $\gamma = 95°$	38.0 ± 0.1	50.9 ± 0.1	(43) (66)	38.7 ± 0.1	26.5 ± 0.3
12	45	55	Lipid tails: $a_T = 4.73$ Å, $\gamma_T = 120°$ Chol monoclinic: $a = 10.50$ Å, $b = 8.40$ Å, $\gamma = 99.7°$ Chol triclinic: $a = b = 14.2$ Å, $\gamma = 96°$	38.8 ± 0.1	50.2 ± 0.1	(43.5) (66.8)	39.9 ± 0.1	29.6 ± 0.3
13	40	60	Lipid tails: $a_T = 4.73$ Å, $\gamma_T = 120°$ Chol triclinic: $a = b = 12.44$ Å, $\gamma = 101°$	38.8 ± 0.1	50.7 ± 0.1	50.63 ± 0.1	41.4 ± 0.1	32.1 ± 0.3
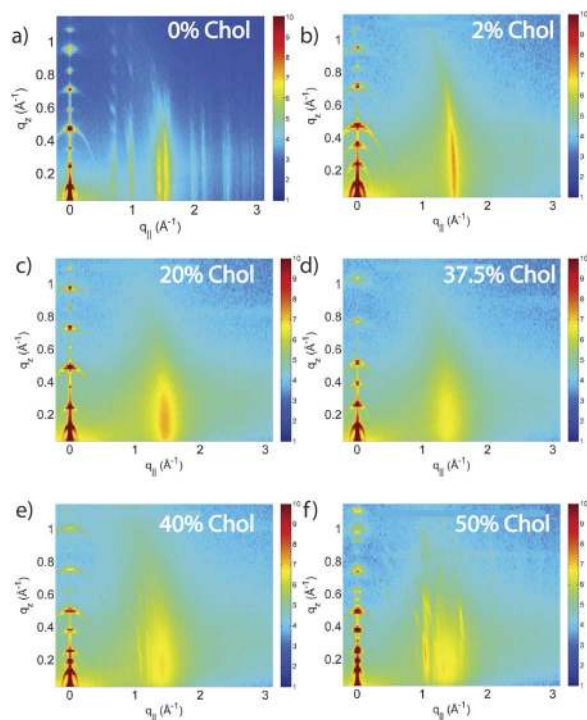
Fig. 2 Two-dimensional X-ray intensity maps of pure DMPC, 2 mol% cholesterol, 20 mol% cholesterol, 37.5 mol% cholesterol, 40 mol% cholesterol, 50 mol% cholesterol (samples 1, 2, 5, 8, 9 and 11, as listed in Table 1). The $q_{\parallel}$ axis probed lateral membrane structure and the perpendicular axis, q_z, probed out-of-plane structure of the multi-lamellar membrane complexes. The pure DMPC sample in (a) showed signals corresponding to the ordering of lipid head groups and lipid tails. Addition of cholesterol resulted in a disordered lateral membrane structure. Additional out-of-plane and in-plane features appeared at cholesterol concentrations above 40 mol%. This was indicative that the molecular packing in the membrane plane changed at this concentration, as well as the topology of the multi-lamellar assembly.

conditions. However, these disordered bilayers do not diffract well (*i.e.* give rise to a limited number of quasi-Bragg peaks), and as such do not lend themselves ideally to traditional crystallographic analysis.

The 100% DMPC sample (Sample 1) in Fig. 2(a) showed a number of well developed in-plane Bragg peaks along the $q_{\parallel}$-axis related to the packing of lipid head groups and lipid tails, as explained in detail in, *e.g.*[34–36] The diffracted intensity has a distinct rod-like shape, typical for a 2-dimensional system. The out-of-plane scattering along q_z showed pronounced and equally spaced Bragg intensities due to the multi-lamellar structure of the membranes, as explained for instance in ref. 37 and 38.

Some qualitative conclusions can be drawn from the 2-dimensional data. The pattern changed by addition of 2 mol% cholesterol in Fig. 2(b): the in-plane scattering showed one pronounced feature, only. The absence of Bragg peaks related to ordering of head groups and tails points to a disordered lateral membrane structure. Higher concentrated samples, such as 37.5 mol% in Fig. 2(d), appeared to be disordered until an ordered pattern with additional intensities was observed at a concentration of 40 mol% cholesterol (Fig. 2(e)). The extra intensities were observed along both out-of-plane and in-plane axes indicated that the molecular packing in the membrane

plane changed at this concentration, as well as the topology of the multi-lamellar assembly.

For a quantitative analysis of the diffracted intensity, the 2-dimensional data were cut along the out-of-plane and in-plane axes. As in-plane features are usually orders of magnitude weaker than the pronounced out-of-plane reflections, slices 0.03 $\text{Å}^{-1} < q_z < 0.3 \text{ Å}^{-1}$ were integrated to enhance the data quality.

Out-of-plane structure and electron densities

The position of the cholesterol molecules in the bilayers was determined from the out-of-plane scans. Data for 0, 30 and 50 mol% cholesterol are shown in Fig. 3 as examples. A series of pronounced and well developed Bragg peaks was observed indicative of a well ordered lamellar structure. Up to 11 Bragg orders could be observed. The pure DMPC sample in Fig. 3 showed small additional peaks, most likely related to defects in the lamellar structure. However, the data in Fig. 3 are presented on a logarithmic scale such that these contributions are 3–4 orders of magnitude weaker than the lamellar peaks. The electron density, ρ_z, was determined from Fourier transformation of the integrated peak intensities, as explained in the Materials and methods section. ρ_z of pure DMPC (Sample 1), and 30 mol% cholesterol (Sample 6) are shown in Fig. 4. The profile for pure DMPC corresponds to a DMPC molecule in the well ordered gel state with both chains in all-trans configuration, as has been reported previously by the Nagle group.[36,39] The electron rich phosphorous group in the head group region can easily be
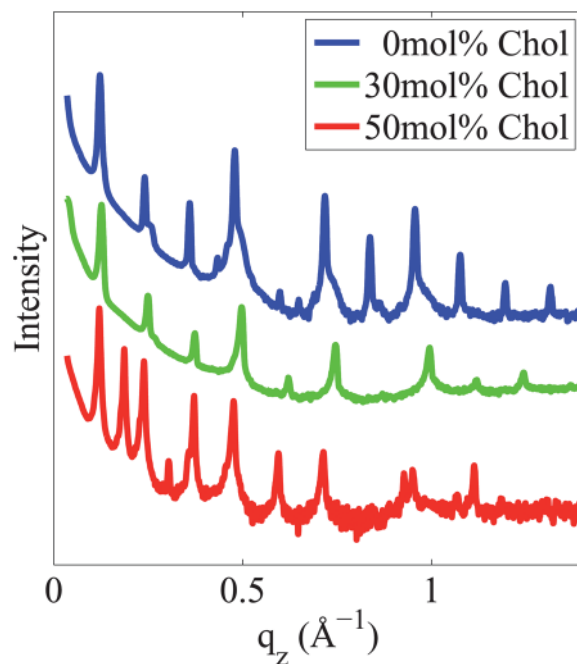

Fig. 3 Out-of-plane data for 0, 30 and 50 mol% cholesterol. Bragg peaks for 0 and 30 mol% can be assigned to lamellar structures with lamellar spacings, d_z of 52.6 and 50.5 Å. Additional Bragg peaks were observed at cholesterol concentrations of 40 mol% and higher. These reflections were indicative of a coexisting lamellar structure with a smaller d_z-spacing of 38.7 Å that was assigned to the formation of a cholesterol bilayer coexisting with the lamellar membrane structure.
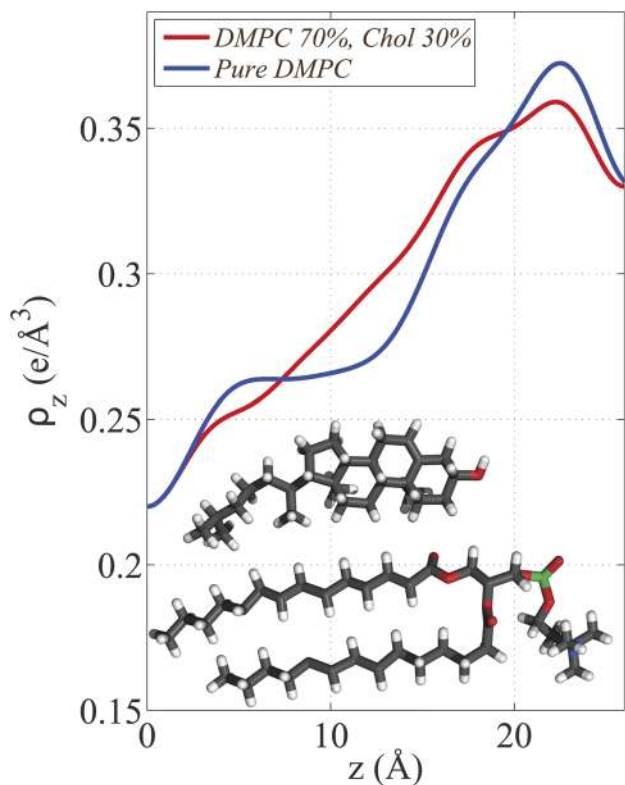
Fig. 4 Electron density profiles of Sample 1 (100 mol% DMPC) and Sample 6 (30 mol% cholesterol). The position of the cholesterol molecule was determined: the hydrophilic oxygen group leads to an increase in electron density at z positions of $\sim$18 Å. The steroid region is found $7\,\text{Å} < z < 16\,\text{Å}$ and the hydrocarbon chain at $2\,\text{Å} < z < 6\,\text{Å}$. As reported previously cholesterol took an upright position in our saturated lipid bilayers with the hydrophilic head pointing towards the aqueous environment. DMPC and cholesterol molecules are drawn to visualize the most likely position and orientations.

identified by the peak in the electron density at $\sim$22 Å. ρ_z monotonically decreases towards the bilayer centre at $z = 0$; only CH_3 groups reside in the centre with an electron density of $\rho(0) = 0.22$ e Å^{-3}.[36,40]

The electron density in the central region of the lipid tails was found to increase in the presence of cholesterol, as shown in Fig. 4. As depicted in the figure, a cholesterol molecule can be fitted at z values of $2\,\text{Å} < z < 19\,\text{Å}$, with the hydrophilic, electron-rich oxygen groups at a z position of $\sim$18 Å. This orientation is compatible with the well known umbrella model[41,42] and "protects" the hydrophobic part of the cholesterol molecule from the aqueous environment, as reported previously for cholesterol in saturated phospholipid bilayers made of DMPC and DPPC.[43,44] The umbrella model suggests[12,13] that cholesterol molecules associate strongly with ordered hydrocarbon chains (usually ones that are fully saturated) in such a manner, that they are shielded from contact with the aqueous environment by the lipid head group. The electron density in Fig. 4 excluded that the cholesterol molecules were lying flat between the two leaflets, as was reported recently for highly unsaturated lipid bilayers.[45,46]

The lamellar spacings, d_z, of the membrane complexes, *i.e.*, the distance between two bilayers in the membrane stack, could be determined from the position of the Bragg peaks in the out-of-

plane data. Results for 0, 30 and 50 mol% cholesterol are shown in Fig. 5. Data are presented as $\sin(\theta)$, the Bragg angle of the lamellar Bragg peaks, as function of the order of the reflection, n. The lamellar spacing was determined from the slope of the lines through the origin, as detailed in the Materials and methods section. A d_z-spacing of 52.6 Å was determined for pure DMPC. The out-of-plane Bragg peaks for low cholesterol content (30 mol % cholesterol is shown in Fig. 5(b)) could be assigned to a single d_z-spacing indicating a well defined lamellar structure of the membrane/cholesterol complexes. Cholesterol concentrations up to 37.5 mol% could be dissolved in the membranes without disturbing the lamellar membrane structure.

Additional out-of-plane Bragg peaks were observed for cholesterol concentrations of 40 mol% and higher. The extra peaks were assigned to a second, smaller d_z-spacing of 38.7 Å, as shown in Fig. 5(c) for 50 mol% cholesterol. This second d_z-spacing is indicative of a cholesterol bilayer coexisting with the lamellar membrane structure, as depicted in Fig. 6(a), as will be discussed below. d_z-spacings for membrane and cholesterol bilayers were determined for all measured complexes (shown in Fig. ESI-2 in the ESI†) and are listed in Table 1.
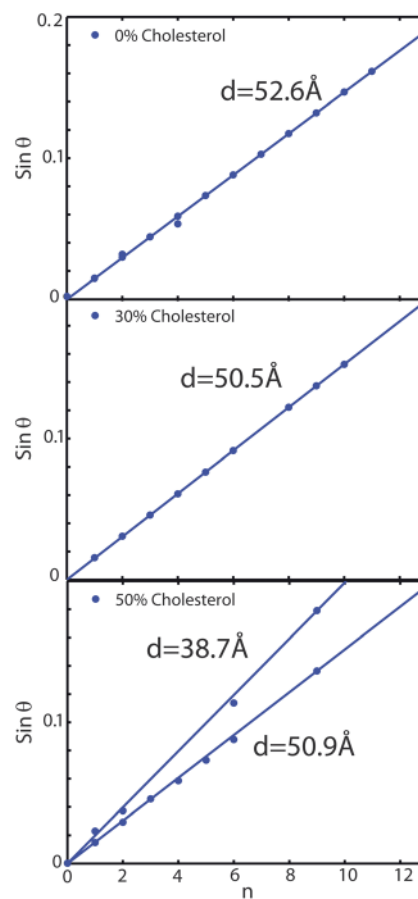

Fig. 5 Peak order of the out-of-plane Bragg peaks, n, from the data in Fig. 3 *vs.* $\sin(\theta)$, where θ is the Bragg angle. The slope of each line shown is inversely proportional to the distance between membranes in the stack, d_z ($\sin(\theta) = \lambda/(2d_z) \times n$). (a) Pure DMPC; (b) DMPC/30 mol% cholesterol (c) DMPC/50 mol% cholesterol. A second, smaller d_z-spacing was observed at concentrations of 40 mol% and higher indicating a coexisting lamellar structure. Values for the different d_z are given in the plots.
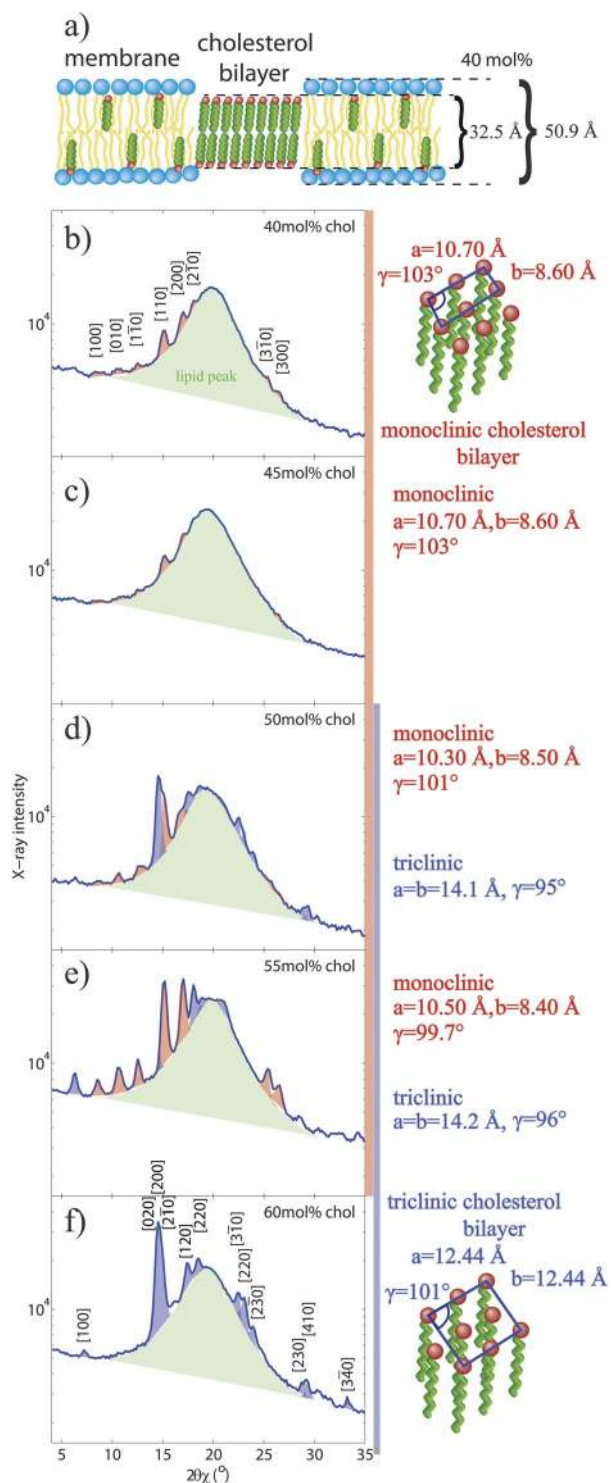
Fig. 6 In-plane scattering of the 40 mol% (b), 45 mol% (c), 50 mol% (d), 55 mol% (e) and 60 mol% (f) complexes (samples 9, 10, 11, 12 and 13), which showed signals due to ordering of the cholesterol molecules. $2\theta\chi$ denotes the in-plane Bragg angle. The hexagonal packing of the lipid tails leads to a broad correlation peak at ~20°. Additional reflections due to ordering of the cholesterol molecules were observed. At 40 mol% the peaks were fit by a monoclinic unit cell. A triclinic structure was observed at the highest concentration of 60 mol%. Monoclinic and triclinic phases were found to coexist at concentrations of 50 and 55 mol%. The cartoon in (a) depicts the molecular arrangement at 40 mol% cholesterol.

In-plane structure

Lateral molecular order of lipids and cholesterol molecules was determined from the in-plane scattering patterns. As discussed in detail in,[34–36] the Bragg peaks in the pure lipid sample could be indexed by an orthorhombic head group lattice (planar space group p2) and a monoclinic unit cell for the lipid tails.

Only one peak was observed at 2 mol% cholesterol in Fig. 2(b). Even at this relatively low concentration (cholesterol : lipids = 1 : 50) the presence of the cholesterol molecules inhibits long-range order of the lipid head groups or tails as evidenced by the absence of Bragg peaks belonging to head or tail unit cells. This is most likely the result of a stochastic distribution of the cholesterol molecules in the bilayer. The area per lipid molecule can be determined when assuming that the lipid tails form a densely packed structure with hexagonal symmetry (planar group p6). The corresponding higher order hexagonal Bragg peaks have also been reported recently by Armstrong et al.[47] The lipid area can then be determined from the position, q_T, of the acyl chain correlation peak to $A_L = 16\pi^2/(\sqrt{3}q_T^2)$.[36,48] From the hexagonal packing, the position of the correlation peak is related to the distance between two acyl tails by $a_T = 4\pi/(\sqrt{3}q_T)$; the area per lipid is calculated to $A_L = \sqrt{3}a_T^2$.

Complexes containing between 2 mol% and 37.5 mol% (Samples 2–8) showed a disordered lateral membrane structure with the lipid tail correlation peak as the only feature; 20 mol% cholesterol and 37.5 mol% are shown as examples in Fig. 2(c) and (d). Several correlation peaks were observed at a cholesterol concentration of 40 mol% in Fig. 2(e). These additional peaks were assigned to ordering of the cholesterol molecules. Because the additional signals occurred simultaneously in the in-plane and out-of-plane data, they were assigned to the structure of cholesterol molecules in coexisting cholesterol bilayer patches.

In-plane diffraction patterns, as extracted from the 2-dimensional data in Fig. 2, for 40, 45, 50, 55 and 60 mol% cholesterol are shown in Fig. 6(b)–(f). Data are presented as function of $2\theta\chi$, the in-plane Bragg angle. The data consist of a broad membrane component, centred at ~20° and a number of additional, narrower Bragg reflections. The molecular structure of the cholesterol molecules in the cholesterol patches could be determined from the additional narrow peaks.

Two types of cholesterol structures were observed in floating lipid/cholesterol films at the air–water interface:[28–30,33] a monoclinic 10×7.5 Å^2 motif and a triclinic, 12.4×12.4 Å^2 motif. The in-plane diffraction data was, therefore, tentatively fit starting from these two motifs. Fitting was done using the Powdercell software package.[49,50] The pattern at 40 mol% cholesterol in Fig. 6(b) was well fit by a monoclinic unit cell with unit cell parameters $a = 10.70$ Å, $b = 8.60$ Å, $\alpha = \beta = 90°$, $\gamma = 103.0°$. The peaks are labeled by their Miller indices, $[hkl]$. A similar diffraction pattern was observed for 45 mol% in Fig. 6(c). Additional peaks were observed at 50 mol% cholesterol in Fig. 6(d). The pattern was well fit by a superposition of the monoclinic motif with parameters $a = 10.30$ Å, $b = 8.50$ Å, $\alpha = \beta = 90°$, $\gamma = 101.0°$ and a triclinic structure with parameters $a = b = 14.10$ Å, $\gamma = 95.0°$ (the values for α and β could not be determined from the data but were taken from[28] to be $\alpha = 91.9°$

and $\beta = 98.1°$). A full list of monoclinic and triclinic reflections with the corresponding Miller indices and in-plane Bragg angle, $2\theta\chi$ are given in Table ESI-1 in the ESI.† The diffraction pattern at 55 mol% in Fig. 6(e) was also well fit by a superposition of monoclinic and triclinic cholesterol structure, until a pure triclinic phase was observed at the highest cholesterol concentration of 60 mol% in Fig. 6(f). The corresponding monoclinic and triclinic unit cells, as suggested in,[28–30] are sketched in Fig. 6. Unit cell parameters and areas per lipid for all complexes are given in Table 1. Note that the monoclinic unit cell contains two cholesterol molecules; the triclinic cell three cholesterol molecules.

Discussion

Molecular structure of the lipid/cholesterol membranes

Cholesterol was found to take an upright orientation, where its hydroxyl group was located near the lipid–water interface in the DMPC bilayers, as reported previously.[43,44] The lamellar spacings of membrane and cholesterol domain together with the areas per lipid and cholesterol molecules could be determined from the analysis of the out-of-plane and in-plane diffraction data, as listed in Table 1. The corresponding data are plotted in Fig. 7. The area per lipid molecule monotonically increased with increasing cholesterol content from ∼41 to ∼48 Å². The d_z spacing showed an increase between 0 mol% and 3 mol% cholesterol. This effect was observed before by the Nagle group[51] as cholesterol was found to reduce the tilt angle of the lipid molecules at small cholesterol concentration, leading to an increased membrane thickness. The lamellar spacing was found to stay constant at cholesterol concentrations between 10 and 30 mol%, until a decrease was observed at 37.5 mol% cholesterol. 37.5 mol% marked the solubility limit of cholesterol in the multi-lamellar DMPC bilayers.

The area per lipid that was determined for the pure DMPC sample can be compared to results published by Tristram-Nagle, Liu, Legleiter and Nagle,[39] who provided a reference for the structure of the gel phase in DMPC membranes. The authors find an area per lipid of ∼47 Å² in fully hydrated bilayers at $T = 10$ °C. The membranes in our study were measured at $T = 20$ °C, however, significantly de-hydrated to 50% RH to enhance structural features. The equilibrated lipid area is governed by a balance of forces resulting from the headgroup and hydrocarbon chains. In the infinitely long chain length regime, where lipid chain–chain van der Waals attractive interactions dominate (i.e., headgroup electrostatic interactions are negligible), the headgroup has a minimum area due to the steric interactions between the interfacial glycerol–carbonyl groups. However, the observed minimal area of ∼41 Å in Fig. 7 is still larger than the optimum packing for all-trans chains of about 40 Å²,[52] indicating that the overall lipid area is determined by the headgroup steric limit.[53]

Additional signals corresponding to coexisting cholesterol phases were observed at a cholesterol concentration of 40 mol%. The lamellar spacing of this phase varied between 41.7 and 38.7 Å for concentrations between 40 and 60 mol% cholesterol. Our interpretation of the out-of-plane data followed the interpretation
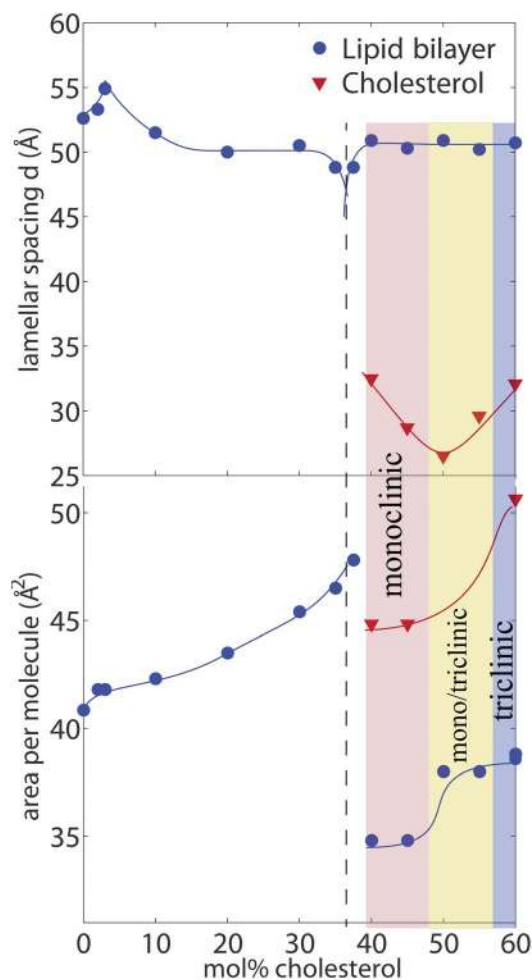

Fig. 7 Lamellar d_z-spacing and area per lipid and cholesterol molecule as determined from the out-of-plane and in-plane data (see Table 1).

by Tulenko, Chen, Mason and Mason[25] and Mason, Tulenko and Jacob.[26] The second, smaller d_z (d_z' in Table 1) spacing was indicative of a coexisting, smaller repeat distance. However, the measured d_z'-spacing of the coexisting cholesterol phase is not directly equivalent to the thicknesses of the cholesterol bilayer. Given the lipid : cholesterol ratio of about 1 : 1, where precipitation was observed, the two most likely scenarios are that a given membrane in the stack is adjacent to (1) another membrane or (2) a cholesterol bilayer. The larger d_z-spacing can, therefore, be assigned and agrees well with the distance between two membranes in the stack. This d_z-spacing is equivalent to the thickness of a bilayer including the water layer that separates neighbouring bilayers in the stack.

The smaller d_z'-spacing involved a bilayer and an adjacent cholesterol bilayer such that $d_z' = \frac{1}{2}d_{lipid} + \frac{1}{2}d_{chol}$, which gives $d_{chol} = 2 \times d_z' - d_{bilayer}$. The corresponding values for d_{chol} vary between 32.5 Å and 26.5 Å and are listed in Table 1. Given the length of a cholesterol molecule of ∼17 Å, these values are compatible with a cholesterol bilayer, where the cholesterol molecules are oriented along the perpendicular z direction, as sketched in Fig. 6(a). The cholesterol molecules were found to

organize laterally in a monoclinic unit cell at 40 mol% cholesterol, which transitioned into a triclinic structure at the highest measured cholesterol concentration of 60 mol%. The area per lipid and cholesterol molecules increased between monoclinic and triclinic phase, with the steepest change at 50 mol% cholesterol, where a coexistence of monoclinic and triclinic cholesterol structure was observed.

Ziblat et al. demonstrated from X-ray diffraction experiments that cholesterol precipitated from bilayers, however, not from monolayers.[54] Yamamoto and Safran[55] recently presented a model that the tilt of the cholesterol molecules may drive phase separation in lipid membranes. Our experiment was not directly sensitive to a possible tilt angle of the cholesterol molecules. However, the lamellar spacing of a cholesterol patch in Table 1 was found to be slightly smaller than the length of two cholesterol molecules, indicative of a tilt of the molecules with respect to the membrane normal. From the decreasing d_z-spacing, the tilt of the cholesterol molecules in the monoclinic phase increased until the triclinic structure formed at the highest cholesterol concentrations.

The addition of cholesterol led to an increase in the area per lipid. We note that the addition of cholesterol to fully hydrated lipid membranes usually leads to a significant decrease of the area per lipid molecule. This is the result of cholesterol's condensation effect, i.e., suppression of fluctuations and ordering of a lipid's hydrocarbon chains.[56,57] As fluctuations were already suppressed in the de-hydrated membrane complexes in this study and the lipid acyl tails in their all-trans configuration, the addition of cholesterol was found to increase the area per lipid molecule as the cholesterol was most likely filling the voids in the lipid structure thereby increasing the distance between lipids.

Edholm and Nagle determined the area per cholesterol molecule in lipid bilayers to be 27 Å^2.[58] The substitution of lipid molecules by cholesterol molecules, which have a smaller area per molecule, leads to the creation of free area in the bilayer. This is observed in Fig. 7 as the area per lipid increased with increasing cholesterol concentrations between 0 and 37.5 mol% cholesterol. The area per cholesterol molecule in the triclinic phase is significantly larger than the area that the cholesterol molecule takes in its monoclinic phase. The general trend in Fig. 7 is that the area per cholesterol molecule increased with increasing cholesterol concentration from 27 Å^2 when the cholesterol is dissolved in the membrane, to ~45 Å^2 in its monoclinic to ~50 Å^2 for cholesterol in its triclinic phase. It can, therefore, be speculated that the formation and size of the coexisting cholesterol bilayers depends on the balance between the area of the membrane and the area of the cholesterol bilayers.

Properties of the cholesterol patches

The size of the cholesterol patches can be estimated from the diffraction experiments. The Scherrer equation[59,60] is often used to determine particle sizes in diffraction experiments. The dimension of the crystalline particle is determined by the equation $L = 0.94\lambda/(B(2\theta)\cos(\theta))$, with $\lambda = 1.5418$ Å the wavelength of the X-rays used, $B(2\theta)$ the width of the correlation peak

in radians, and θ the diffraction angle at which the peak is observed. The X-ray setup used in this paper was optimized for intensity at the cost of a relaxed $q_\parallel$ resolution and was, therefore, not optimized for the precise determination of peak widths. However, applying Scherrer's equation to the monoclinic [110] reflection at 55 mol% cholesterol in Fig. 6(e) with a resolution corrected width (FWHM) of 0.19° in $2\theta\chi$ and a $\theta\chi$-position of ~8° results in an approximate size of the cholesterol patches of L ~450 Å.

In the umbrella model,[41,42] each lipid head group can "host" two cholesterol molecules, thus shielding the mostly hydrophobic cholesterol molecule from the aqueous environment. Based on this model the maximum theoretical solubility of cholesterol in saturated lipid bilayers is determined to be 66 mol% cholesterol.[41,61] In the neighbourhood of this point, critical fluctuations will prevail and the correlation length describing local dynamic domain formation can get very large,[62,63] which can lead to the formation of immiscible domains at concentrations before the maximum solubility is reached, as discussed in a recent review.[62]

The existence of transient nanometer sized lipid domains was recently reported experimentally by Armstrong et al.[47] Coherence length dependent neutron diffraction experiments performed in fluid dipalmitoylphosphatidylcholine (DPPC)/cholesterol membranes containing 32.5 mol% cholesterol revealed the existence of highly ordered lipid domains in equilibrium with a disordered matrix. The lipids in these domains were found to be in a gel-like state and to be saturated with cholesterol molecules (66 mol%, in agreement with the umbrella model). Dynamic cholesterol structures were also reported by Meinhardt, Vink and Schmid[64] from computer simulations in dipalmitoylphosphatidylcholine (DPPC)/cholesterol. These dynamic heterogeneities are most likely precursors for the formation of the immiscible domains observed in Fig. 6.

The membrane complexes in this study were at a low hydration to emphasize structural features in the X-ray diffraction experiments and obtain a high spatial resolution. Dynamics, such as undulations, are highly suppressed in this state. We can, therefore, not make a statement about a potential role of undulations in the formation of the cholesterol domains.

The occurrence of immiscible cholesterol plaques at high cholesterol concentrations was also checked at higher relative humidities, closer to physiological conditions (shown in Fig. ESI-1 in the ESI†). While the additional signals corresponding to the coexisting immiscible cholesterol phase in the 40 mol% sample disappeared with increasing hydration of the membrane complexes, signals corresponding to cholesterol plaques were found to exist at higher cholesterol concentration under full hydration of the membranes. It can, therefore, be speculated that immiscible cholesterol plaques can form in saturated lipid bilayers under physiological conditions at cholesterol concentrations of more than 40 mol%.

Conclusion

We determined the structure of highly oriented, multi-lamellar solid supported dimyristoylphosphatidylcholine (DMPC)

membranes containing up to 60 mol% of cholesterol. The lamellar spacing d_z of the model membranes and the area per lipid and cholesterol molecule were determined from 2-dimensional X-ray measurements. The maximum solubility of cholesterol in saturated lipid membranes was determined to be 37.5 mol%.

We present direct experimental evidence for the formation of immiscible cholesterol plaques at cholesterol concentrations of more than 40 mol% cholesterol, coexisting with the lamellar membrane structure. The cholesterol molecules were found to form bilayers with a monoclinic structure at 40 mol% cholesterol, which transitioned into a triclinic structure at the highest cholesterol concentration of 60 mol%.

Materials and methods

Preparation of the highly-oriented multi-lamellar membrane samples

Highly oriented multi-lamellar membranes were prepared on single-side polished silicon wafers. 100 mm diameter, 300 μm thick silicon (100) wafers were pre-cut into 2 × 2 cm² chips. 1,2-dimyristoyl-sn-glycero-3-phosphocholine (DMPC), and cholesterol (depicted in Fig. 1 (a)) were mixed in different ratios and dissolved in a 1 : 1 chloroform/2,2,2-trifluoroethanol (TFE) solution at a concentration of 15 mg ml⁻¹. The lipid solution did not spread well on ultrasonic-cleaned wafers and de-wetted during drying. The silicon substrates were, therefore, cleaned in a piranha acid solution made of 98% concentrated H_2SO_4 and 30% concentrated H_2O_2 at a ratio of 3 : 1 by volume. Wafers were placed in this solution, covered with parafilm and heated to 298 K for 30 minutes. This treatment removes all organic contamination and leaves the substrates in a hydrophilic state. We used silanization to cover the silicon surface through self-assembly with organo-functional alkoxysilane molecules (APTES). The organic part of the APTES molecules was found to provide a perfect hydrophobic interface for the formation of the biological tissue. The 1 : 1 mix of chloroform–TFE, which was used to dissolve lipids and chloroform, is a non-polar solvent. In order for the solvent to spread well and cover the whole substrate uniformly, the silicon wafers were made hydrophobic to match the solvent properties. A 1% (by volume) solution of APTES and 99% ethanol was prepared. The wafers were immersed in the APTES solution and covered with parafilm, heated to 298 K and placed on a tilting incubator (20 speed, 3 tilt) for 12 hours. The tilting incubator creates a circular flow in the beaker to ensure an even APTES distribution and prevent buildup on the surface of the wafers. The wafers were then placed in a clean pyrex dish and annealed in vacuum at 388 K for 3 hours to create a uniform coverage of the APTES molecules on the surface.[65] Each wafer was thoroughly rinsed three times by alternating with ~50 mL of ultra pure water and methanol. The tilting incubator was heated to 313 K and the lipid solution was placed inside to equilibrate. The wafers were rinsed in methanol, dried with nitrogen gas and placed in the incubator. 200 μL of lipid solution was applied on each wafer, and the wafers covered with a Petri dish to let the solvent evaporate slowly to allow time for the membranes to form. Wafers were tilted during the drying process for 30 minutes (speed 15, tilt 1) such that the lipid solution spread evenly on the wafers. After drying, the samples were placed in vacuum at 313 K for 12 hours to remove all traces of the solvent. The bilayers were annealed and rehydrated before use in a saturated K_2SO_4 solution which provides ~98% relative humidity (RH). The hydration container was allowed to equilibrate at 293 K in an incubator. The temperature of the incubator was then increased gradually from 293 K to 303 K over a period of ~5 hours to slowly anneal the multi-lamellar structure. This procedure results in highly oriented multi-lamellar membrane stacks and a uniform coverage of the silicon substrates. About 3000 highly oriented stacked membranes with a thickness of ~10 μm are produced using this protocol. The samples were stored in a refrigerator at 5 °C and heated to 55 °C for 1 h before scanning to erase a possible thermal history. This procedure in particular destroys possible crystalline L_C or sub-gel phases that may form during storage at low temperatures and low hydration.[66] The high sample quality and high degree of order is necessary to determine in-plane and out-of-plane structure of the membranes and the position of the cholesterol molecules. Table 1 lists all samples prepared for this study.

X-ray scattering experiment

Out-of-plane and in-plane X-ray scattering data was obtained using the Biological Large Angle Diffraction Experiment (BLADE) in the Laboratory for Membrane and Protein Dynamics at McMaster University. BLADE uses a 9 kW (45 kV, 200 mA) CuKα Rigaku Smartlab rotating anode at a wavelength of 1.5418 Å. Both source and detector are mounted on movable arms such that the membranes stay horizontal during the measurements. Focussing multi-layer optics provides a high intensity parallel beam with monochromatic X-ray intensities up to 10^{10} counts/(s × mm²). This beam geometry provides optimal illumination of the solid supported membrane samples to maximize the scattering signal. All data were obtained in grazing incidence, small and wide angle scattering geometry. A sketch of the scattering geometry is shown in Fig. 1(c). By using highly oriented membrane stacks, the in-plane ($q_\parallel$) and out-of-plane (q_z) structure of the membranes could be determined. From the high resolution X-ray diffraction experiments we determine the molecular structure of the membranes in two different ways: (1) the out-of-plane membrane structure to determine the location of the different molecules in the membrane with sub-nanometer resolution and (2) the lateral organization of the different molecular components in the plane of the membrane. The result of such an X-ray experiment is a 2-dimensional intensity map of a large area (0.03 Å⁻¹ < q_z < 1.1 Å⁻¹ and 0 Å⁻¹ < $q_\parallel$ < 3.1 Å⁻¹) of the reciprocal space. All scans were measured at 20 °C and 50% relative humidity. The samples were kept in a so-called humidity chamber during the measurements. Temperature was controlled by a water bath to better than 0.1 °C; the humidity inside the chamber was controlled by using a saturated salt solution of $Mg(NO_3)_2$. Structural features are more pronounced in dry samples as fluctuations, which lead to attenuation and smearing of Bragg peaks, are strongly suppressed.

Out-of-plane structure and electron densities

The out-of-plane structure of the membranes was determined using specular reflectivity, see, *e.g.* ref. 36–38. The electron density, $\rho(z)$, is approximated by a 1D Fourier analysis:[39]

$$\rho(z) = \rho_W + \frac{F(0)}{d_z} + \frac{2}{d_z} \sum_{n=1}^{N} F(q_n) \nu_n \cos(q_n z)$$
$$= \rho_W + \frac{F(0)}{d_z} + \frac{2}{d_z} \sum_{n=1}^{N} \sqrt{I_n q_n} \nu_n \cos\left(\frac{2\pi n z}{d_z}\right) \quad (1)$$

N is the highest order of the Bragg peaks observed in the experiment and ρ_W the electron density of bulk water. The integrated peak intensities, I_n, are multiplied by q_n to receive the form factors, $F(q_n)$.[67,68] The bilayer form factor $F(q_z)$, which is in general a complex quantity, is real-valued in the case of centrosymmetry. The phase problem of crystallography, therefore, simplifies to the sign problem $F(q_z) = \pm|F(q_z)|$. And the phases, ν_n, can only take the values ±1. The phases ν_n are needed to reconstruct the electron density profile from the scattering data following eqn (1). When the membrane form factor $F(q_z)$ is measured at several q_z values, a continuous function, $T(q_z)$, which is proportional to $F(q_z)$, can be fitted to the data:[67–70]

$$T(q_z) = \sum_n \sqrt{I_n q_n} \, \text{sinc}(\pi d_z q_z - \pi n). \quad (2)$$

Once an analytical expression for $T(q_z)$ has been determined from fitting the experimental peak intensities, the phases ν_n can be determined from $T(q_z)$.

In order to put ρ_z on an absolute scale, the electron densities were scaled to fulfil the condition $\rho(0) = 0.22$ e Å^{-3} (the electron density of a CH_3 group) in the centre of the bilayer, and $\rho(d_z/2) = 0.33$ e Å^{-3} (the electron density of water, ρ_W) outside the bilayers.

$T(q)$ was fit to the experimentally determined peak intensities using eqn (2) to determine an array of phases ν_n out of the corresponding 2^{10} combinations of ±1. All samples were well fit by the phase array $[\bar{1}11\bar{1}\bar{1}\bar{1}\bar{1}\bar{1}\bar{1}]$. The integrated intensity of the out-of-plane Bragg peaks is used to calculate the electron density profile perpendicular to the bilayers following eqn (1). Fig. 4 shows data of Sample 1 (pure DMPC) and Sample 6 containing 30 mol% cholesterol as an example.

The d_z-spacing between two neighbouring membranes in the stack was determined from the distance between the well developed Bragg reflections ($d_z = 2\pi/\Delta q_z$) along the out-of-plane axis, q_z, as shown in Fig. 3. The peaks were well fit by Gaussian peak profiles. To assign the peaks to different phases, Bragg's law can be re-written as $\sin(\theta) = \lambda/(2d_z) \times n$. By plotting the sine of the Bragg angles *versus* the order of the different Bragg reflections, $\sin(\theta(n))$ *vs.* n, peaks which belong to the same d_z-spacing fall on a straight line through the origin, whose slope is proportional to $1/d_z$. The corresponding data are shown in Fig. 5 for selected concentrations; data for all concentrations are included in the ESI.† Up to a peak order n of 12 was observed in the out-of-plane data. Note that not all diffraction orders are necessarily observed for the different d_z-spacings as their scattering intensity depends on the form factor of the bilayers and oscillates between zero and maximum intensity as a function of q_z.

Acknowledgements

References

1 A. Ridsdale, M. Denis, P.-Y. Gougeon, J. K. Ngsee, J. F. Presley and X. Zha, *Mol. Biol. Cell*, 2006, **17**, 1593.
2 O. G. Mouritsen, *Life-as a matter of fat: the emerging science of lipidomics*, Springer, 2005.
3 K. E. Bloch, *Crit. Rev. Biochem. Mol. Biol.*, 1983, **14**, 47–92.
4 P. L. Yeagle, *Biochim. Biophys. Acta, Biomembr.*, 1985, **815**, 33–36.
5 D. E. Vance and H. Van den Bosch, *Biochim. Biophys. Acta, Mol. Cell Biol. Lipids*, 2000, **1529**, 1–8.
6 A. Chaudhuri and A. Chattopadhyay, *Biochim. Biophys. Acta, Biomembr.*, 2011, **1808**, 19–25.
7 K. Simons and E. Ikonen, *Nature*, 1997, **387**, 569572.
8 K. Simons and E. Ikonen, *Science*, 2000, **290**, 1721–1726.
9 D. M. Engelman, *Nature*, 2005, **438**, 578–580.
10 P. S. Niemelä, S. Ollila, M. T. Hyvnen, M. Karttunen and I. Vattulainen, *PLoS Comput. Biol.*, 2007, **3**, e34.
11 D. A. Brown and E. London, *J. Biol. Chem.*, 2000, **275**, 17221.
12 R. Petrie, P. Schnetkamp, K. Patel, M. Awasthi-Kalia and J. Deans, *J. Immunol.*, 2000, **165**, 1220.
13 B. Papanikolaou, A. Papafotika, C. Murphy, T. Papamarcaki, O. Tsolas, M. Drab, T. V. Kurzchalia, M. Kasper and S. Christoforidis, *J. Biol. Chem.*, 2005, **28**, 26406.
14 L. Pike, *J. Lipid Res.*, 2006, **47**, 1597.
15 L. Pike, *J. Lipid Res.*, 2009, **50**, S323.
16 D. Lingwood and K. Simons, *Science*, 2009, **327**, 4650.
17 C. Eggeling, C. Ringemann, R. Medda, G. Schwarzmann, K. Sandhoff, S. Polyakova, V. N. Belov, B. Hein, C. von Middendorf, A. Schönle and S. W. Hell, *Nature*, 2009, **457**, 1159–1162.
18 F. G. van der Goot and T. Harder, *Semin. Immunol.*, 2001, **13**, 89–97.
19 P.-F. Lenne and A. Nicolas, *Soft Matter*, 2009, **5**, 2841–2848.
20 T. Apajalahti, P. Niemelä, P. N. Govindan, M. S. Miettinen, E. Salonen, S.-J. Marrink and I. Vattulainen, *Faraday Discuss.*, 2009, 2010.
21 E. Watkins, C. Millerb, J. Majewski and T. Kuhl, *Proc. Natl. Acad. Sci. U. S. A.*, 2011, **108**, 6975–6980.
22 A. Hall, T. Róg, M. Karttunen and I. Vattulainen, *J. Phys. Chem. B*, 2010, **114**, 7797–7807.
23 K. Simons and M. J. Gerl, *Nat. Rev. Mol. Cell Biol.*, 2010, **11**, 688–699.
24 M. C. Rheinstädter and O. G. Mouritsen, *Curr. Opin. Colloid Interface Sci.*, 2013, **18**, 440–447.
25 T. N. Tulenko, M. Chen, P. E. Mason and R. P. Mason, *J. Lipid Res.*, 1998, **39**, 947–956.

26 R. P. Mason, T. N. Tulenko and R. F. Jacob, *Biochim. Biophys. Acta, Biomembr.*, 2003, **1610**, 198–207.

27 M. Raguz, L. Mainali, J. Widomska and W. K. Subczynski, *Biochim. Biophys. Acta, Biomembr.*, 2011, **1808**, 1072–1080.

28 H. Rapaport, I. Kuzmenko, S. Lafont, K. Kjaer, P. B. Howes, J. Als-Nielsen, M. Lahav and L. Leiserowitz, *Biophys. J.*, 2001, **81**, 2729–2736.

29 I. Solomonov, M. J. Weygand, K. Kjaer, H. Rapaport and L. Leiserowitz, *Biophys. J.*, 2005, **88**, 1809–1817.

30 I. Solomonov, J. Daillant, G. Fragneto, K. Kjaer, J. Micha, F. Rieutord and L. Leiserowitz, *Eur. Phys. J. E: Soft Matter Biol. Phys.*, 2009, **30**, 215–221.

31 R. Ziblat, L. Leiserowitz and L. Addadi, *J. Am. Chem. Soc.*, 2010, **132**, 9920–9927.

32 R. Ziblat, L. Leiserowitz and L. Addadi, *Angew. Chem., Int. Ed.*, 2011, **50**, 3620–3629.

33 R. Ziblat, I. Fargion, L. Leiserowitz and L. Addadi, *Biophys. J.*, 2012, **103**, 255–264.

34 J. Katsaras, V. A. Raghunathan, E. J. Dufourc and J. Dufourcq, *Biochemistry*, 1995, **34**, 4684–4688.

35 V. A. Raghunathan and J. Katsaras, *Phys. Rev. Lett.*, 1995, **74**, 4456–4459.

36 M. A. Barrett, S. Zheng, G. Roshankar, R. J. Alsop, R. K. Belanger, C. Huynh, N. Kučerka and M. C. Rheinstädter, *PLoS One*, 2012, **7**, e34357.

37 G. Pabst, N. Kučerka, M.-P. Nieh, M. Rheinstädter and J. Katsaras, *Chem. Phys. Lipids*, 2010, **163**, 460–479.

38 G. Fragneto and M. Rheinstädter, *C. R. Phys.*, 2007, **8**, 865–883.

39 S. Tristram-Nagle, Y. Liu, J. Legleiter and J. F. Nagle, *Biophys. J.*, 2002, **83**, 3324–3335.

40 L. Toppozini, C. L. Armstrong, M. A. Barrett, S. Zheng, L. Luo, H. Nanda, V. Garcia Sakai and M. Rheinstädter, *Soft Matter*, 2012, **8**, 11839–11849.

41 J. Huang and G. W. Feigenson, *Biophys. J.*, 1999, **76**, 2142–2157.

42 J. Dai, M. Alwarawrah and J. Huang, *J. Phys. Chem. B*, 2010, **114**, 840–848.

43 A. Léonard, C. Escrive, M. Laguerre, E. Pebay-Peyroula, W. Néri, T. Pott, J. Katsaras and E. J. Dufourc, *Langmuir*, 2001, **17**, 2019.

44 C. L. Armstrong, M. A. Barrett, A. Hiess, T. Salditt, J. Katsaras, A.-C. Shi and M. C. Rheinstädter, *Eur. Biophys. J.*, 2012, **41**, 901–913.

45 N. Kučerka, D. Marquardt, T. Harroun, M.-P. Nieh, S. Wassall and J. Katsaras, *J. Am. Chem. Soc.*, 2009, **131**, 16358.

46 N. Kučerka, D. Marquardt, T. Harroun, M.-P. Nieh, S. Wassall, D. de Jong, L. Schäfer, S. Marrink and J. Katsaras, *Biochemistry*, 2010, **49**, 7485.

47 C. L. Armstrong, D. Marquardt, H. Dies, N. Kučerka, Z. Yamani, T. A. Harroun, J. Katsaras, A.-C. Shi and M. C. Rheinstädter, *PLoS One*, 2013, **8**, e66162.

48 T. T. Mills, G. E. S. Toombes, S. Tristram-Nagle, D.-M. Smilgies, G. W. Feigenson and J. F. Nagle, *Biophys. J.*, 2008, **95**, 669–681.

49 W. Kraus and G. Nolze, *J. Appl. Crystallogr.*, 1996, **29**, 301–303.

50 http://www.ccp14.ac.uk/ccp/web-mirrors/powdcell/a_v/v_1/powder/e_cell.html, 2000.

51 T. Mills, J. Huang, G. Feigenson and J. Nagle, *Gen. Physiol. Biophys.*, 2009, **28**, 126–139.

52 H. Petrache, S. Dodd and M. Brown, *Biophys. J.*, 2000, **79**, 3172–3192.

53 J. Pan, F. A. Heberle, S. Tristram-Nagle, M. Szymanski, M. Koepfinger, J. Katsarasa and N. Kučerka, *Biochim. Biophys. Acta, Biomembr.*, 2012, **1818**, 2135–2148.

54 R. Ziblat, K. Kjaer, L. Leiserowitz and L. Addadi, *Angew. Chem., Int. Ed.*, 2009, **48**, 8958–8961.

55 T. Yamamoto and S. A. Safran, *Soft Matter*, 2012, **8**, 5439–5442.

56 F. de Meyer and B. Smit, *Proc. Natl. Acad. Sci. U. S. A.*, 2009, **106**, 3654–3658.

57 F. J.-M. de Meyer, A. Benjamini, J. M. Rodgers, Y. Misteli and B. Smit, *J. Phys. Chem. B*, 2010, **114**, 10451–10461.

58 O. Edholm and J. F. Nagle, *Biophys. J.*, 2005, **89**, 1827–1832.

59 P. Scherrer, *Göttinger Nachrichten Math. Phys.*, 1918, **2**, 98–100.

60 U. Holzwarth and N. Gibson, *Nat. Nanotechnol.*, 2011, **6**, 534.

61 J. Huang, J. T. Buboltz and G. W. Feigenson, *Biochim. Biophys. Acta, Biomembr.*, 1999, **1417**, 89–100.

62 A. R. Honerkamp-Smith, S. L. Veatch and S. L. Keller, *Biochim. Biophys. Acta, Biomembr.*, 2009, **1788**, 53–63.

63 J. Risbo, M. Sperotto and O. G. M. Mouritsen, *J. Chem. Phys.*, 1995, **103**, 3643–3656.

64 S. Meinhardt, R. L. C. Vink and F. Schmid, *Proc. Natl. Acad. Sci. U. S. A.*, 2013, **110**, 4476–4481.

65 E. T. Vandenberg, L. Bertilsson, B. Liedberg, K. Uvdal, R. Erlandsson, H. Elwing and I. Lundström, *J. Colloid Interface Sci.*, 1991, **147**, 103–118.

66 H. W. Meyer, K. Semmler, W. Rettig, W. Pohle, A. S. Ulrich, S. Grage, C. Selle and P. J. Quinn, *Chem. Phys. Lipids*, 2000, **105**, 149–166.

67 J. F. Nagle and M. C. Wiener, *Biophys. J.*, 1989, **55**, 309–313.

68 J. Nagle, R. Zhang, S. Tristram-Nagle, W. Sun, H. Petrache and R. Suter, *Biophys. J.*, 1996, **70**, 1419–1431.

69 G. I. King and C. R. Worthington, *Phys. Lett. A*, 1971, **35**, 259–260.

70 T. Adachi, *Chem. Phys. Lipids*, 2000, **107**, 93–97.